Supplementary material for: Long tails in deep columns of natural and anthropogenic tropospheric tracers

J. David Neelin, Benjamin R. Lintner, Baijun Tian, Qinbin Li, Li Zhang, Prabir K. Patra, Moustafa T. Chahine, and Samuel N. Stechmann

1 Relationship of atmospheric applications and forced passive tracer problems

1.1 Examples from prototype problems

For reference, we review selected aspects of prior work on idealized prototype problems that informs the observational and modeling analysis here. Tracer distributions with long, approximately exponential tails were first noted experimentally in Rayleigh-Bénard convection and in a stirred fluid with a maintained temperature gradient [*Heslot et al.*, 1987; *Castaing et al.*, 1989; *Lane et al.*, 1993; *Gollub et al.*, 1991]. This motivated exploration in simplified analytic or numerical settings [e.g., *Pumir et al.*, 1991; *Shraiman and Siggia*, 1994; *Pierrehumbert*, 1994, 2000; *Ngan and Pierrehumbert*, 2000].

The idealization of a specified, constant gradient $\bar{q}_z$ in one direction z, with flow properties constant in that direction used in *Bourlioux and Majda* [2002, BM02 hereafter] yields for the forced solutions of Eq. 1 of the main text

$$\partial_t q + \mathbf{v} \cdot \nabla q - \kappa \nabla^2 q = w \bar{q}_z \qquad (1)$$

When non-dimensionalized by length and velocity scales L, V, the explicit parameter is the Peclet number $Pe = VL/\kappa$. Other important parameters controlling the distribution are implicit in the characteristics of the advecting flow. Here we illustrate with z identified with the vertical direction which is directly relevant to creating the deep columns of tracer. Application to a region of horizontal gradient is discussed below.

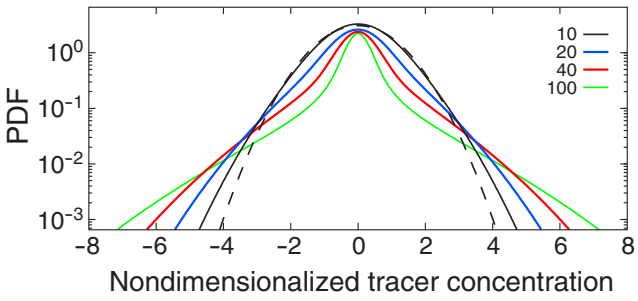

Figure 1: Distribution from the prototype forced advection-diffusion problem by *Bourlioux and Majda* [2002], showing Peclet number dependence for Pe=10, 20, 40, 100. Dashed lines show a Gaussian with the same standard deviation as for Pe=10.

An instructive example from BM02. The solutions are for a two-dimensional case of Eq. 1, with the velocity field

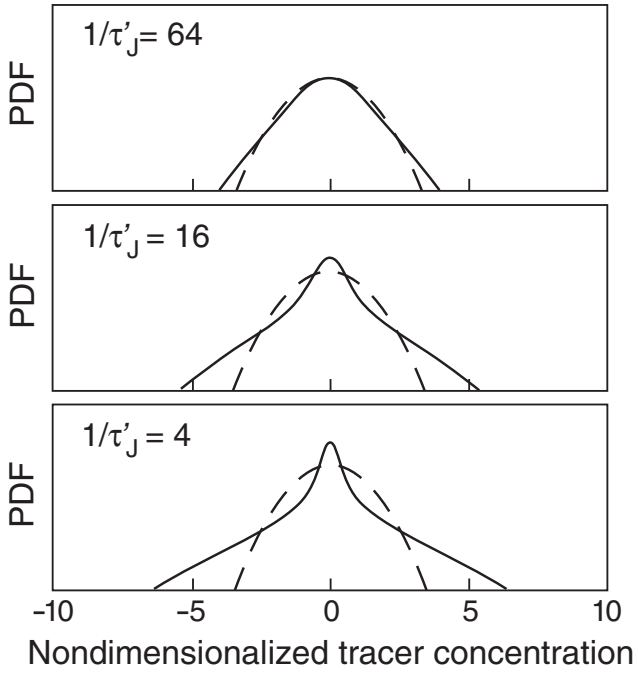

Figure 2: Distribution from the prototype forced advection-diffusion problem by Bourlioux and Majda, showing their case with Peclet number 1000 for three different nondimensional autocorrelation times τ'_J for a Gaussian random process in the flow field in the direction of the gradient. For shorter autocorrelation times the tails become steeper and eventually approach Gaussian (dashed lines show a Gaussian with the same standard deviation). Reprinted with permission from *Bourlioux and Majda* [2002]. Copyright Physics of Fluids, 2002, American Institute of Physics.

in the direction perpendicular to the gradient ("horizontal" $\mathbf{v}$ in the setup described above) varying sinusoidally in time, constant in space, while the velocity in the direction of the gradient ("vertical" w above) is sinusoidal in space and an autocorrelated Gaussian random process in time. Figure 1 shows a sequence as a function of Peclet number, choosing a range in which the distribution evolves from slightly broader than Gaussian to having stretched exponential tails that flair out a distinct angle from the core. The tails for Pe= 100 are beginning to resemble the asymptotic case that is approached for high Peclet number. Solved by the same methods as BM02, for parameters corresponding to their figure 5, this case provides a reference for considerations of asymmetry in the distribution below. In developing intuition for examination of observed

cases, one should not associate the shapes in the example shown solely with the Peclet number, since characteristics of the flow field can strongly affect which shape occurs for a given Peclet number.

Figure 2 shows how the relationship between tails and core changes as the autocorrelation time of the velocity decreases, in the regime BM02 refer to as weakly intermittent. They identify the physical mechanism producing the tails as occurrences of long excursions in the direction of the gradient when streamlines are not blocked by the cross flow. The tails are affected by additional parameters, for example, the period of the crosswind; and from Eq. 1, the distribution scales with the magnitude of both the gradient and the w variations. In atmospheric applications, the analogs of these quantities are internally determined, and can differ not only between models and observations, but between different tracers as the sources produce dominant gradients in different locations and directions in an inhomogeneous, anisotropic flow. The effect of autocorrelation time on the tails in Figure 2 is relevant to both of these situations: models with parameterized vertical transport are often less intermittent in vertical velocity; and tracers such as water vapor where the vertical gradient dominates (as shown in Figure 1b of the main text) will be affected by vertical motions with shorter autocorrelation times than is typical for synoptic scale horizontal transports affecting tracers with strong horizontal gradients.

Earlier cases examined numerically by *Pierrehumbert* [2000] and *Ngan and Pierrehumbert* [2000] show that distributions with qualitatively similar core and tail characteristics can be obtained for various inhomogeneous and intermittent forcings. In particular, for a forcing consisting of several randomized Fourier modes, a series of distributions similar to the examples in Figures 1 and 2 can be constructed as a function of the autocorrelation time of the forcing [*Ngan and Pierrehumbert*, 2000]. Furthermore, in two-dimensional advection along isentropic surfaces such distributions can be simulated for stratospheric flows despite such complexities as mixing barriers [*Hu and Pierrehumbert*, 2001, 2002]. It is from the work of Pierrehumbert and collaborators that we first became aware of forced passive-tracer advection problems as a means of generating long tails. We follow their usage of the term long tail as a shorthand to describe these longer-than-Gaussian, approximately exponential or stretched exponential tails (i.e., these are not heavy-tailed distributions). These references provide additional discussion of tail-generating mechanisms beyond the simple case summarized here.

In addition to the aforementioned tails of exponential and stretched exponential types, power law tails have been observed in vertical differences of such quantities as horizontal velocity and potential temperature in atmospheric soundings [*Schertzer and Lovejoy*, 1985], and they have been interpreted in terms of multifractals and multiplicative cascade models [*Schertzer and Lovejoy*, 1991], [*Lovejoy et al.*, 2009].

1.2 Considerations for atmospheric flow conditions

1.2.1 Straightforward extensions of prototypes

Some simple considerations relevant to relating the prototypes to situations more applicable to troposphere transports are outlined here, focusing first on the vertical gradient case (for discussion of horizontal gradients, see sections 1.2.3 and 2.2).

Example 1: Weak vertical structure. Consider modifying the BM02 assumptions to include slow vertical variations in vertical velocity $w(\epsilon z)$. If one can neglect an order ϵ term due to vertical variations of $\mathbf{v}$ in horizontal advection, and an order ϵ^2 term in vertical diffusion, then the forced solution in q simply reflects the vertical structure in w, and these deep structures are governed by the BM02 equation.

Example 2: Build-up of tracer due to unbalanced surface flux. The case of a surface flux F not balanced by a sink in the interior of the atmosphere (as for CO_2) is equivalent when the resulting trend is removed to a source-sink problem with a effective interior sink that maintains a vertical gradient against the surface input. Averaging Eq. 1 of the main text over the domain in the absence of interior sink S yields a linear increase of the domain-average concentration $\langle q \rangle$ by F

$$\partial_t \langle q \rangle = \langle F \rangle \tag{2}$$

Subtracting this from Eq. 1 of the main text and defining $q' = q - \langle q \rangle$ and an effective sink $S_F = \langle F \rangle$ gives a tracer equation for departures from a long-term build up

$$\partial_t q' + \mathbf{v} \cdot \nabla q' + w \partial_z q' - \kappa \nabla^2 q' - \partial_z \kappa_v \partial_z q' = -S_F \tag{3}$$

Example 3: Surface boundary layer. Consider a source of tracer via a surface flux, with vertical turbulent diffusion keeping q constant through the lower atmospheric boundary layer (ABL), from the surface at z=0 to ABL top at z_b, above which the turbulent flux becomes small relative to the vertical advection. The vertical velocity increases rapidly through the ABL, and for illustration we approximate it as independent of the vertical coordinate for $z > z_b$. Vertically integrating Eq. 1 of the main text, with $\hat{q}$ denoting the vertical integral then gives

$$\partial_t \hat{q} + \mathbf{v} \cdot \nabla \hat{q} - \kappa \nabla^2 \hat{q} = w q_b^+ \tag{4}$$

where q_b^+ is the value just above the ABL top (where vertical diffusive flux is neglected). For upward motion, q_b^+ is given by the boundary layer value q_b. For extended periods of downward motion, this value can be driven to lower values from above, yielding one source of asymmetry between ascent and descent. In the approximation that q_b^+ is constant, with suitable simplifications of velocity spatial and time dependence, Eq. 4 reduces to Eq. 1 examined by BM02. We can thus anticipate that many of their results can provide qualitative guidance for analyzing distributions of column tracers, with the caveat of possible asymmetry between upward and downward motion discussed below.

1.2.2 Asymmetry in tracer distributions

Asymmetries between the positive and negative tails of the distribution are seen in both observations and models for realistic atmospheric conditions, whereas the simple prototypes are typically examined for symmetric cases. For vertical advection, two obvious sources of asymmetry are asymmetry in the intensity of upward and downward motions, and the role of the boundary layer. Each can be related to the simple prototypes.

Small modifications to the BM02 forced advection-diffusion problem illustrate how flow field characteristics can produce asymmetry in the distribution. Figure 3 shows a case for Pe=20 similar to Figure 1 but modified by inclusion of a deterministic flow field. This contribution to w is given by the sum of two Fourier modes in x with phase chosen such that velocity in the gradient direction toward lower tracer has a more intense maximum, mimicking more localized intense upward motion and widespread, slower downward motion for a tracer with downward vertical gradient such as water vapor. This velocity component is added to the single-mode random component of Figure 1. The asymmetry in intensity of "upward/downward" motion affects the size of the anomalies produced when streamlines experience long excursions in the direction of the gradient. For the case shown, this is a longer positive tail, akin to that for column water vapor in Figure 1 of the main text.

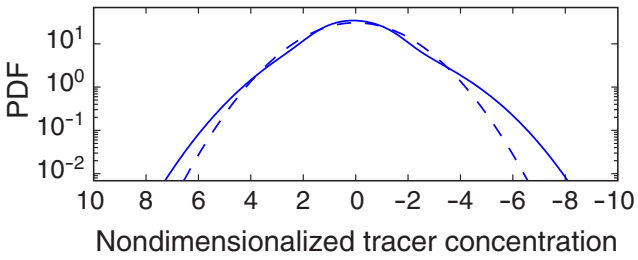

Figure 3: Distribution from the prototype forced advection-diffusion problem with flow field modified to produce asymmetry. Dashed lines show a Gaussian with the same standard deviation as each case.

An illustration of asymmetry to the atmospheric boundary layer interacting with vertical advection starts from Example 3 discussed above. Parameterize the q_b^+ dependence in Eq. 4 as $f(\hat{q})q_b$, with $f = 1$ for $\hat{q}$ outside some modest neighborhood of zero, and $f \to 0$ as $\hat{q} \to 0$. The low concentration tail would then be limited when approaching zero values of free-tropospheric concentrations. Positing that this can be approximately mapped onto the BM02 solution q, try $\hat{q} = g(q)(q_b/\bar{q}_z)$ in Eq. 4. If one can neglect a term of the form $d^2g/dq^2\kappa(\partial_x q)^2$ (easily satisfied for most of the range, heuristically justified for large negative q and small κ), then Eq. 4 transforms to (1) provided $dg/dq = f(g(q))$. For $f = 1$, $\hat{q}$ is linearly related to the BM02 solution q, implying the same distribution over the upper range. For suitable f, the large negative values of q are mapped onto a range above zero in $\hat{q}$, implying an asymmetry that cuts off the low-concentration tail. This provides a more detailed heuristic justification of the claim that BM02 can provide a close prototype for column integrated (or column-integrated above the ABL) tracer, even for circumstances where a maintained gradient is replaced by a forced boundary layer. The low-end cut off is qualitatively similar to that seen in instantaneous water vapor observations of high spatial resolution in Figure 1 of the main text.

1.2.3 Vertical and horizontal gradients

Realistic tropospheric tracer sources will tend to maintain both vertical and horizontal gradients of the tracer. Furthermore, the gradients within the fluid will strongly depend on the flow pattern, the lifetime of the tracer compared to advective time scales, the configuration of the surface source and other factors. It is thus somewhat surprising that prototypes based on two-dimensional flow with a fixed gradient provide as useful a prototype for tropospheric tracer distributions as the observations in the main text suggest. The stratospheric case on isentropic surfaces [*Hu and Pierrehumbert*, 2001, 2002; *Hu*, 2007] bears a more obvious relation to two-dimensional prototypes. Two situations in the troposphere may lend themselves to comparable simplicity. First, when a strong vertical gradient is maintained as discussed above, which the observational results suggest holds well for the case of tropical water vapor anomalies. Second, when a horizontal gradient is maintained on scales such that a long-lived tracer tends to be lofted through a deep layer. The two-dimensional problem then roughly applies in the horizontal. We provide an example of this in the section 2.2 for an idealized tracer with infinite lifetime. For tracers of intermediate lifetime or comparable importance of horizontal versus vertical gradients, the typical configuration of the tracer anomalies may be much more complex, but provided a gradient is maintained, the results suggest that the processes are sufficiently similar to yield comparable distributions. Clearly it will be of interest to quantify this in future work.

1.2.4 Turbulent diffusivity and horizontal scale of the observations

The molecular diffusivity for air would give very large Peclet number, so when considering the model data comparisons here, it is worth emphasizing that horizontal and vertical averages (both inherent to the instrument and explicit) of the observations imply that the relevant diffusion-like process is by turbulent eddies. Filaments of tracer twisted up by the flow at scales smaller than the observation scale will only be seen by their effects on the average. Models account for the effects of subgrid-scale turbulent mixing through various diffusion schemes, often of higher order, e.g., biharmonic with $\kappa_{bi} \sim 10^{15}\mathrm{m}^4\mathrm{s}^{-1}$. Under such a scheme, the equivalent of the Peclet number is $Pe_{bi} \sim \frac{vL^3}{\kappa_{bi}}$. At a spatial scale of $\sim 2.5°$, for realistic

windspeeds (i.e., $V \sim 5\text{ms}^{-1}$), Pe_{bi} is of order 10^2. This corresponds to a diffusive time scale on the order of 100 days compared to an advective timescale on the order of 1 day. While it is not always easy to estimate a specific number for a given model, many modern models likely have a comparable separation of these timescales to capture filamentary structures. The examples in section 1.1 suggest this is sufficient to yield very broad tails for some flow configurations, with factors such as the autocorrelation time of the velocity field in the region and direction of the strong gradients for a given tracer affecting the precise distribution.

2 Other tracers

2.1 NO_x and ozone

Figure 4 presents distributions of NO_x and ozone from Geos-Chem simulations as a further indication that broader than Gaussian tails will be ubiquitous, while the details of the distribution change sufficiently from tracer to tracer to potentially provide interesting validation targets. NO_x and ozone are more complex than the tracers considered in the main text in that they have interior sources as well as sinks. In the upper troposphere, ozone has a downward vertical gradient.

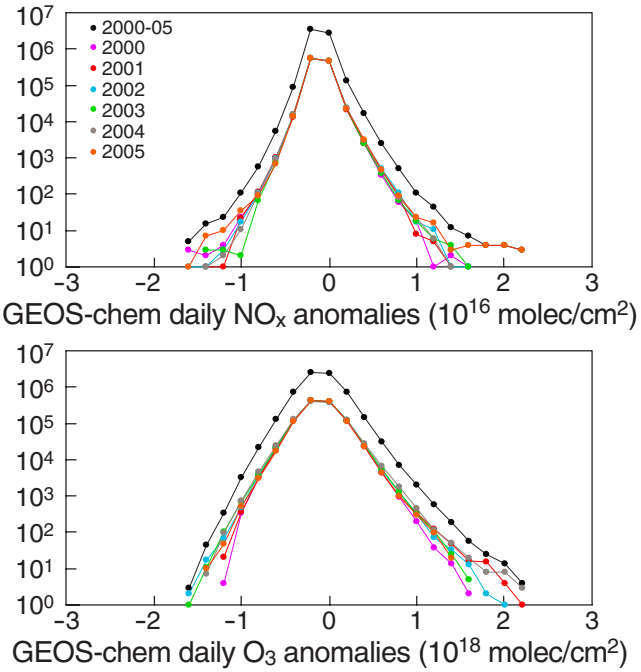

Figure 4: Distribution (black dots) for 2000-2005 for tropical points (20S-20N) of column-integrated anomalies of (a) NO_x; (b) ozone. Distributions for individual years are given by colored dots.

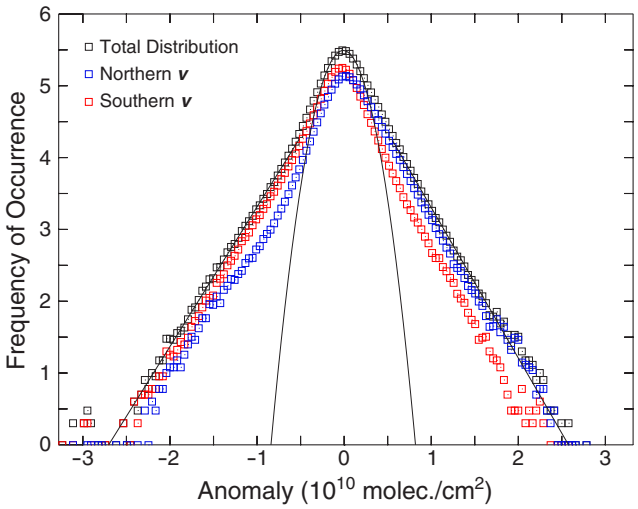

Figure 5: Distribution (black squares) for the tropics (20S-20N) of column-integrated anomalies of an idealized tracer with surface of source in a narrow strip at mid-latitudes simulated in an atmospheric chemistry model (see text). Cases for lower tropospheric (1000-500 mb average) velocities southward/northward are shown in blue/red.

2.2 Idealized forcing in an atmospheric chemistry transport model

To partially address the gap between prototype problems and observations or simulations for complex atmospheric situations, we have also analyzed distributions for tracers with simplified sources and sinks, but in a realistic atmospheric flow. The Center for Climate System Research/National Institute for Environmental Studies/ Frontier Research Center for Global Change (CCSR/NIES/-FRCGC ACTM) atmospheric general circulation model-driven Chemistry-Transport Model (hereafter ACTM) *Numaguti et al.* [1997]; *Patra et al.* [2009] at 2.8 degrees resolution is used. ACTM meteorological fields are nudged toward NCEP/DOE AMIP-II Reanalysis (from January, 1st 2000-December 31st, 2005) at T42 truncation in the horizontal and 32 vertical sigma-pressure levels up to ∼50 km in the vertical. In these idealized-source experiments, tracer input by surface fluxes is constant in a specified latitude band, zero elsewhere. There is no sink of tracer, but the time-trend of the tracer concentration is removed before analysis, as discussed above.

Here we choose an example that highlights the role that horizontal advection can play for the case of a long-lived tracer with forcing that introduces strong horizontal gradients. Figure 5 shows a case with surface flux input in narrow mid-latitude strip at 40N; this case may be viewed as a simplified prototype for atmospheric input by industrialized nations of long-lived tracers such as carbon dioxide or SF_6.

The distribution of daily average anomalies over 20S-20N exhibits exponential tails and a narrow Gaussian core. The leading effect of the horizontal gradient for this example may be seen by dividing the distribution into subsets

associated with northward/southward horizontal velocity. The positive tail of the full distribution is seen to be associated with southward motion from the regions of high concentration in the northern hemisphere. Despite the more complex process in which the tracer is both lofted to create deep column loadings near the source region, and advected horizontally across the resulting gradient, the long, roughly exponential tails are still clearly seen.

References

Bourlioux, A., and A. J. Majda, Elementary models with probability distribution function intermittency for passive scalars with a mean gradient, *Physics of Fluids*, *14*, 881–897, doi:10.1063/1.1430736, 2002.

Castaing, B., G. Gunaratne, F. Heslot, L. Kadanoff, A. Libchaber, S. Thomae, X. W. adn S. Zaleski, and G. Zanetti, Scaling of hard thermal turbulence in Rayleigh-Bénard convection, *J. Fluid Mech.*, *204*, 1–30, doi:10.1017/S0022112089001643, 1989.

Gollub, J. P., J. Clarke, M. Gharib, B. Lane, and O. N. Mesquita, Fluctuations and transport in a stirred fluid with a mean gradient, *Phys. Rev. Lett.*, *67*(25), 3507–3510, doi:10.1103/PhysRevLett.67.3507, 1991.

Heslot, F., B. Castaing, and A. Libchaber, Transitions to turbulence in helium gas, *Phys. Rev. A*, *36*(12), 5870–5873, doi:10.1103/PhysRevA.36.5870, 1987.

Hu, Y., Probability distribution function of a forced passive tracer in the lower stratosphere, *Advances in Atmos. Sci.*, *24*, 1–18, 2007.

Hu, Y., and R. T. Pierrehumbert, The advection-diffusion problem for stratospheric flow. Part I: Concentration probability distribution function, *J. Atmos. Sci.*, *58*, 1493–1510, 2001.

Hu, Y., and R. T. Pierrehumbert, The advection-diffusion problem for stratospheric flow. Part II: Concentration probability distribution function of tracer gradients, *J. Atmos. Sci.*, *59*, 2830–2845, 2002.

Lane, B. R., O. N. Mesquita, S. R. Meyers, and J. P. Gollub, Probability distributions and thermal transport in a turbulent grid flow, *Phys. Fluids A*, *5*, 2255, doi:10.1063/1.858564, 1993.

Lovejoy, S., A. F. Tuck, S. J. Hovde, and D. Schertzer, Vertical cascade structure of the atmosphere and multifractal dropsonde outages, *J. Geophys. Res.*, *114*, D07,111, doi:10.1029/2008JD010651, 2009.

Ngan, K., and R. T. Pierrehumbert, Spatially correlated and inhomogeneous random advection, *Physics of Fluids*, *12*(4), 822–834, doi:10.1063/1.870338, 2000.

Numaguti, A., M. Takahashi, T. Nakajima, and A. Sumi, Development of CCSR/NIES atmospheric general circulation model, *CGER's Supercomput, Monogr. Rep.,*, *3*, 1–48, 1997.

Patra, P. K., M. Takigawa, G. S. Dutton, K. Uhse, K. Ishijima, B. R. Lintner, K. Miyazaki, and J. W. Elkins, Transport mechanisms for synotpic, seasonal, and interannual SF_6 variations and age of air in the troposphere, *Atmos. Chem. Phys.*, *9*, 1209–1225, 2009.

Pierrehumbert, R. T., Tracer microstructure in the large-eddy dominated regime, *Chaos, Solitons and Fractals*, *4*, 1994.

Pierrehumbert, R. T., Lattice models of advection-diffusion, *Chaos: An Interdisciplinary Journal of Nonlinear Science*, *10*(1), 61–74, doi:10.1063/1.166476, 2000.

Pumir, A., B. I. Shraiman, and E. D. Siggia, Exponential tails and random advection, *Phys. Rev. Lett.*, *66*, 2984–2987, doi:10.1103/PhysRevLett.66.2984, 1991.

Schertzer, D., and S. Lovejoy, The dimension and intermittency of atmospheric dynamics, in *Turbulent Shear Flows 4*, edited by B. Launder, pp. 7–33, Springer, New York, 1985.

Schertzer, D., and S. Lovejoy, *Nonlinear Variability in Geophysics: Scaling and Fractals*, 512 pp., Kluwer Academic, Dordecht, 1991.

Shraiman, B. I., and E. D. Siggia, Lagrangian path integrals and fluctuations in random flow, *Phys. Rev. E*, *49*, 2912–2927, doi:10.1103/PhysRevE.49.2912, 1994.